Jet dynamics in topographically-forced shallow-water planetary atmospheres

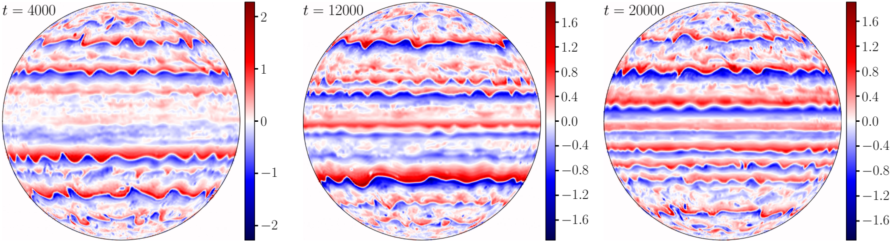

David Dritschel, Mahdi Jalali & Richard Scott

University of St Andrews

Kyoto, November 2024

A brief history

AUGUST 1978 GARETH P. WILLIAMS 1399

Planetary Circulations: 1. Barotropic Representation of Jovian and Terrestrial Turbulence

GARETH P. WILLIAMS

Geophysical Fluid Dynamics Laboratory/NOAA, Princeton University, Princeton, NJ 08540

(Manuscript received 2 December 1975, in final form 13 April 1978)

Streamfunction ψ at early times, here 4.6 and 23 days.

$\Delta\psi = 40\mathrm{km}^2/\mathrm{s}$.

1422 JOURNAL OF THE ATMOSPHERIC SCIENCES VOLUME 35

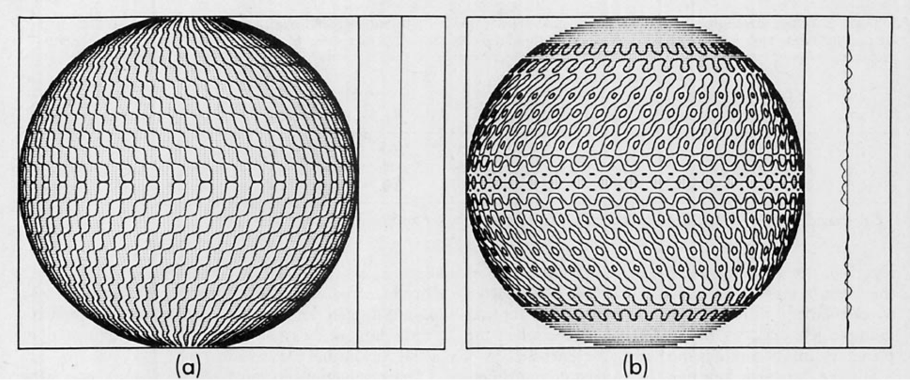

Streamfunction ψ at late times, here 161 and 294.4 days.

$\Delta\psi = 80\text{km}^2/\text{s}$.

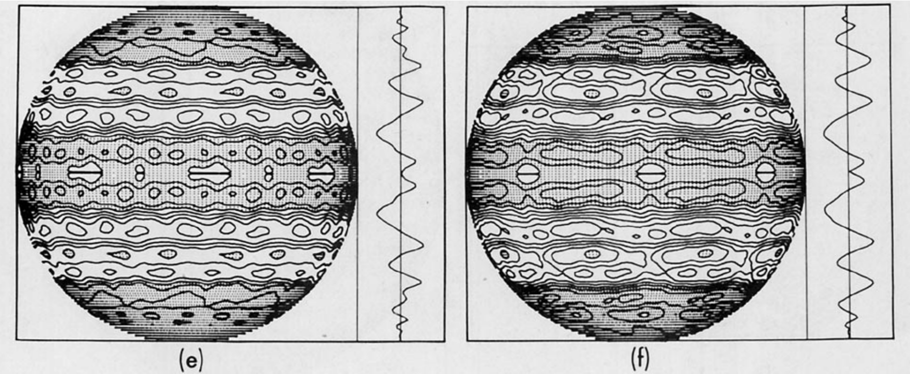

FIG. 16. Case J2. Streamfunction at days (a) 4.6, (b) 23.0, (c) 46.0, (d) 73.3, (e) 161, (f) 294.4. $u^* = 100$ m s^{-1}, (a)–(d) $\Delta\psi = 40$ km^2 s^{-1}, (e)–(f) $\Delta\psi = 80$ km^2 s^{-1}. Computational sector is repeated for global display. A cine version of this solution is available.

Spherical shallow-water simulations of Jovian vortices

VOL. 41, NO. 4 JOURNAL OF THE ATMOSPHERIC SCIENCES 15 FEBRUARY 1984

Geostrophic Regimes, Intermediate Solitary Vortices and Jovian Eddies

GARETH P. WILLIAMS

Geophysical Fluid Dynamics Laboratory/NOAA, Princeton University, Princeton, NJ 08540

TOSHIO YAMAGATA[1]

Geophysical Fluid Dynamics Program, Princeton University, Princeton, NJ 08540

(Manuscript received 12 April 1983, in final form 25 October 1983)

Spherical shallow-water simulations of Jovian vortices

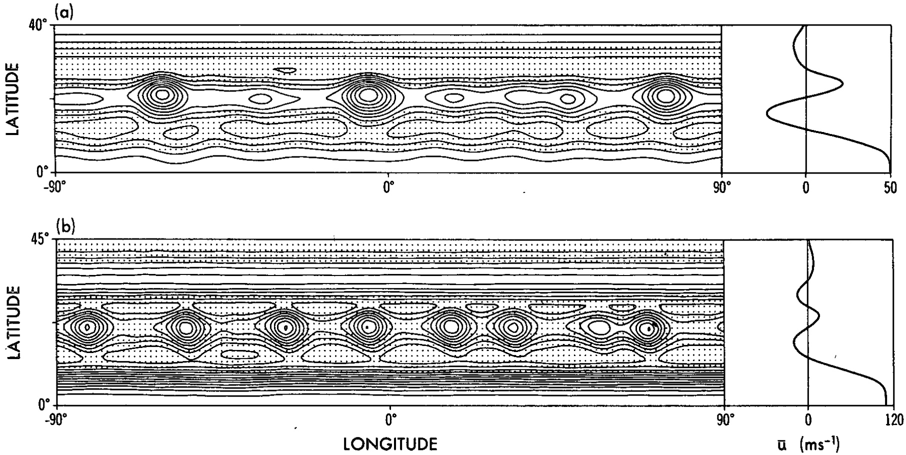

FIG. 16. Solution SW7 and SW8. Anticyclonic vortices produced by (a) moderately, and (b) strongly, unstable anticyclonic shear zones. Contour interval for the free-surface variable $\eta(\lambda, \theta)$ is (a) 1.5 km and (b) 1 km; negative values are shaded. Jovian parameter values are as in Section 2f, with (a) $g = g_J/12$, (b) $g = g_J/10$ and with $\tau = 5 \times 10^6$ s and $\nu = 0.1$ km^2 s^{-1}. Profiles on the rhs give the latitudinal distribution of the zonally averaged zonal flow, with scales of (a) ± 50 m s^{-1} and (b) ± 120 m s^{-1}.

Forced-dissipative spherical shallow-water turbulence

3158 JOURNAL OF THE ATMOSPHERIC SCIENCES VOLUME 64

SPECIAL
Jets and Annular Structures in Geophysical Fluids
COLLECTION

Forced-Dissipative Shallow-Water Turbulence on the Sphere and the Atmospheric Circulation of the Giant Planets

R. K. SCOTT

Northwest Research Associates, Inc., Bellevue, Washington

L. M. POLVANI

Department of Applied Physics and Applied Mathematics, Columbia University, New York, New York

(Manuscript received 8 May 2006, in final form 18 January 2007)

ABSTRACT

Although possibly the simplest model for the atmospheres of the giant planets, the turbulent forced-dissipative shallow-water system in spherical geometry has not, to date, been investigated; the present study aims to fill this gap. Unlike the freely decaying shallow-water system described by Cho and Polvani,

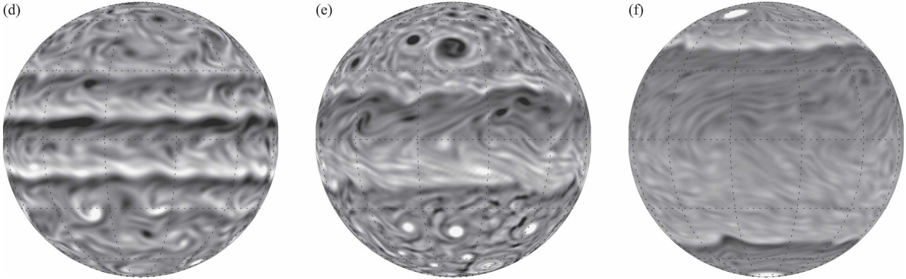

FIG. 14. (a)–(c) Potential vorticity and (d)–(f) vorticity for the three simulations with planetary parameters: (left) Jupiter, (middle) Saturn, and (right) Uranus/Neptune. Shading is same as in Fig. 9.

From Scott & Polvani (2007), §4a:

Our forcing is designed to represent the actual forcing of the giant planetary atmospheres by overturning convective systems or other random motions generated by the deep turbulent interior. There is very little known about these processes and so a simple set of assumptions is required. Keeping these to a minimum, we suppose that the forcing is random in space and time; uniform, homogeneous, and isotropic in space; and induces motions primarily at scales smaller than those of the dominant features of the atmospheres. For

SPECIAL
Jets and Annular Structures in Geophysical Fluids
COLLECTION

Numerical Simulations of Forced Shallow-Water Turbulence: Effects of Moist Convection on the Large-Scale Circulation of Jupiter and Saturn

ADAM P. SHOWMAN

The University of Arizona, Tucson, Arizona

(Manuscript received 15 June 2006, in final form 6 December 2006)

ABSTRACT

To test the hypothesis that the zonal jets on Jupiter and Saturn result from energy injected by thunderstorms into the cloud layer, forced-dissipative numerical simulations of the shallow-water equations in spherical geometry are presented. The forcing consists of sporadic, isolated circular mass pulses intended to represent thunderstorms; the damping, representing radiation, removes mass evenly from the layer. These

Equatorial jet emergence with Newtonian cooling

1466 JOURNAL OF THE ATMOSPHERIC SCIENCES VOLUME 72

Mechanism for the Formation of Equatorial Superrotation in Forced Shallow-Water Turbulence with Newtonian Cooling

IZUMI SAITO AND KEIICHI ISHIOKA

Division of Earth and Planetary Sciences, Graduate School of Science, Kyoto University, Kyoto, Japan

(Manuscript received 12 August 2014, in final form 13 November 2014)

Prograde or retrograde?

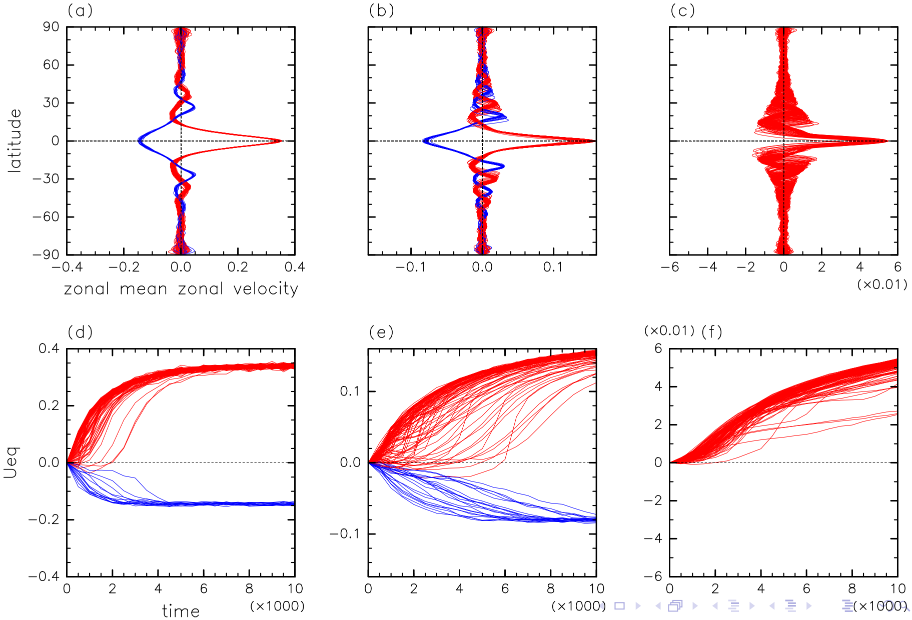

The physical model

We use the shallow-water equations on a rotating, spherical planet:

$$\frac{\mathrm{D}\boldsymbol{u}}{\mathrm{D}t} + 2\boldsymbol{\Omega} \times \boldsymbol{u} = -g\boldsymbol{\nabla}(h+b)$$

$$\frac{\partial h}{\partial t} + \boldsymbol{\nabla} \cdot (h\boldsymbol{u}) = -\frac{h-H}{\tau}$$

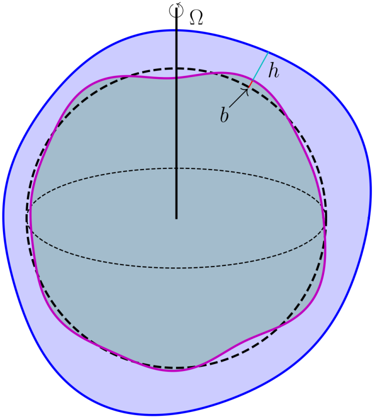

where b is the specified time-dependent "topography", H is the constant mean layer thickness, and τ is the thermal damping rate.
All other symbols are standard.

Image from https://upload.wikimedia.org/wikipedia/commons

The "topographic" forcing b is intended to model convective forcing from below in the giant gas planets, due e.g. to thunderstorms, following Showman (2007) and Thomson & McIntyre (2016).

Here, we consider a time-correlated random field b composed of a set of spherical harmonics $Y_n^m(\phi, \lambda)$. We examine both narrow-band ($n \in [30, 34]$) and broad-band ($n \in [1, 72]$) forcing.

A flat spectrum (in order n) is used for narrow-band forcing, while a spectrum $S(n) \propto \xi e^{-\xi}$ with $\xi \equiv (n/k_b)^3$ with $k_b = 32$ is used for broad-band forcing.

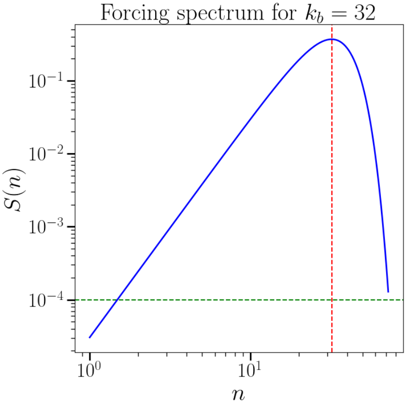

The thermal relaxation (or Newtonian cooling), $-(h-H)/\tau$, in the height equation is a simple model of radiative damping. The height anomaly is $h - H \propto \theta'$, i.e. the potential temperature anomaly in SW theory.

This form of damping is argued to be more relevant than (frictional) Ekman damping for the gas giants (Thomson & McIntyre, 2016).

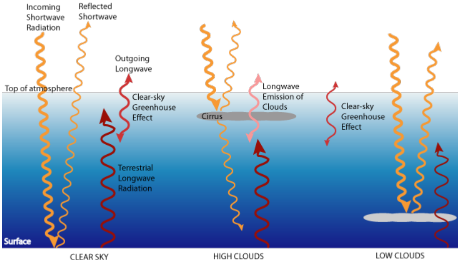

https://commons.wikimedia.org/wiki

Note that gravity g can be combined with H to define a short-scale gravity-wave speed $c = \sqrt{gH}$, if we recast the equations using the dimensionless height anomaly $\tilde{h} = (h-H)/H$ and topography $\tilde{b} = b/H$.

Moreover we are free to scale all lengths by the radius a of the planet, and all times by the planetary rotation period Ω.

This is tantamount to taking $a = 1$ and $\Omega = 2\pi$.

The remaining model parameters are:

- the Rossby deformation wavenumber, $k_D \equiv 2\Omega/c$,
- the thermal relaxation time-scale, τ,
- the amplitude of the topographic forcing, b_{rms}, and
- the forcing de-correlation time-scale, t_b.

For the forcing, $\tilde{b}$, we follow Scott & Polvani (2007). After every time step (of length Δt), we first create a random field, α, scaled so its r.m.s. value is b_{rms}. We then redefine $\tilde{b}$ as $C(\mu\tilde{b} + \sqrt{1-\mu^2}\,\alpha)$, where $\mu = 1 - \Delta t/t_b$ and C ensures the r.m.s. value of the new $\tilde{b}$ is still b_{rms}.

$\tilde{b}(\boldsymbol{x}, t)$ at three times; top: narrow band, bottom: broad band

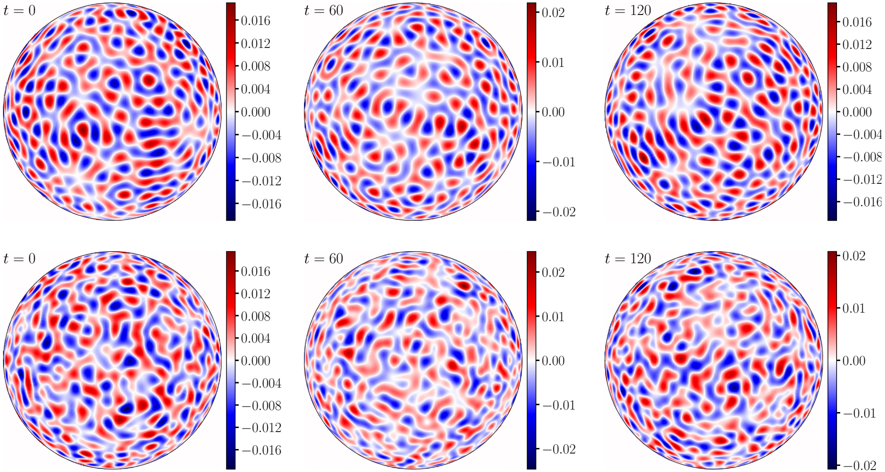

Parameters: $b_{\rm rms} = 0.005$ and $t_b = 50$. Equatorial view.

The numerical model

We use the Combined Lagrangian Advection Method (CLAM) where the potential vorticity (PV)

$$q = \frac{\zeta + f}{1 + \tilde{h}} \qquad (f = 2\Omega \sin\phi)$$

has both a contour and a grid representation (Dritschel & Fontane, 2010).

A regular $n_g \times 2n_g$ latitude-longitude grid is employed, with latitudes

$$\phi_j = (j - 1/2)\pi/n_g - \pi/2\,,$$

$j = 1, 2, \ldots, n_g$, that avoid the poles (Mohebalhojeh & Dritschel, 2007).

FFTs are used in longitude, while 4th-order compact differences are used in latitude (or FFTs around great circles).

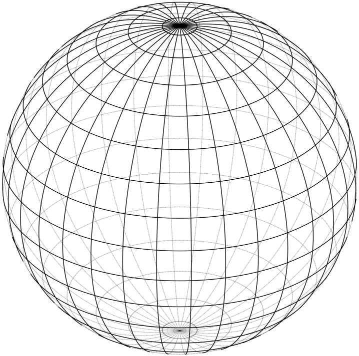

Alongside PV, we employ the divergence $\delta = \boldsymbol{\nabla} \cdot \boldsymbol{u}$ and the acceleration divergence $\gamma = \boldsymbol{\nabla} \cdot (\mathrm{D}\boldsymbol{u}/\mathrm{D}t)$ in place of $\tilde{h}$ and $\boldsymbol{u} = (u, v)$:

$$\frac{\mathrm{D}q}{\mathrm{D}t} = S\,, \qquad \frac{\partial \delta}{\partial t} = \gamma + \text{NL terms}, \qquad \frac{\partial \gamma}{\partial t} = c^2 \nabla^2 \delta + \text{NL terms}.$$

This significantly improves the accuracy of representing the balanced, PV-controlled dynamics, *and* the residual imbalance, or gravity waves (Mohebalhojeh & Dritschel, 2000–2016).

We initialise the flow using $q(\boldsymbol{x}, 0) = f$ and the nonlinear balance relations $\partial\delta/\partial t = \partial\gamma/\partial t = 0$ to define the initial fields of δ and γ.

The corresponding $\tilde{h}$ and $\boldsymbol{u}$ fields — at any time — are found by inverting the definitions of q, δ and γ.

Simulation results

We have investigated the following parameter variations:

- $k_D = 1, 5, 25,$
- $\tau = 100, 500, 2500,$
- $b_{\text{rms}} = 0.001, 0.005, 0.025,$
- $t_b = 10, 50, 250.$

Note that $k_D \sim 10$ to 40 is thought to appropriate for the gas giants. The other parameters are much less well known.

All simulations use a basic grid resolution of $n_g \times 2n_g = 256 \times 512$, though the effective resolution is <u>much</u> higher (Dritschel & Tobias, 2012).

Simulations are run until $t = 10000 + 40\tau$ days, using a gravity-wave resolving time-step $\Delta t = 0.8\Delta\phi/c$, where $\Delta\phi = \pi/n_g$.

Effect of forcing spectrum

$\zeta(\boldsymbol{x}, t)$ at three times; top: narrow band, bottom: broad band

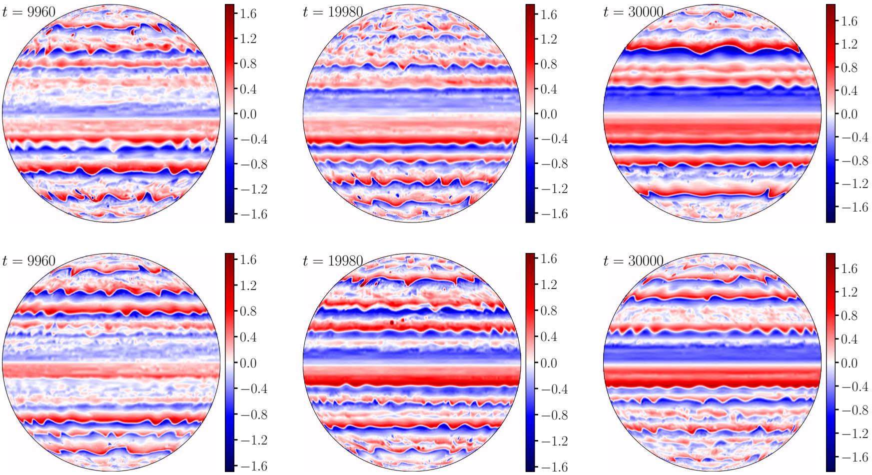

$k_D = 25$, $\tau = 500$, $b_{\text{rms}} = 0.005$, $t_b = 50$

$\zeta(\boldsymbol{x}, t)$ at three times; top: narrow band, bottom: broad band

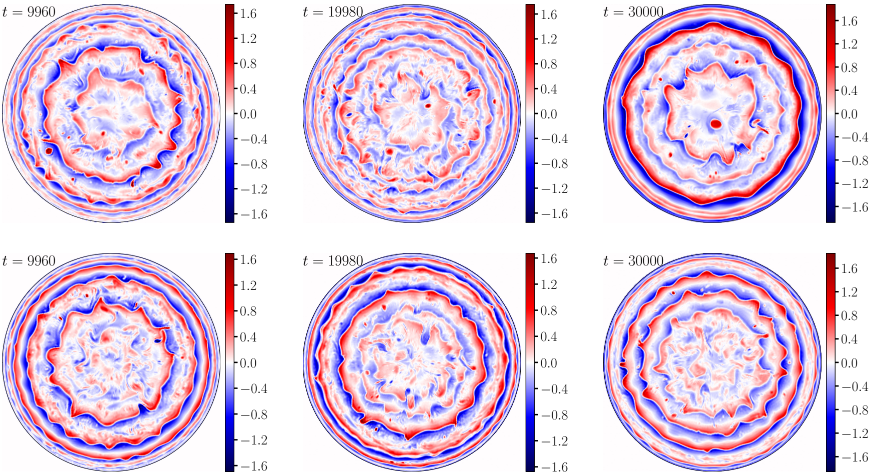

$k_D = 25, \ \ \tau = 500, \ \ b_{\text{rms}} = 0.005, \ \ t_b = 50$

$\bar{u}(t,\phi)$ $\qquad$ $\partial\bar{q}/\partial\phi(t,\phi)$

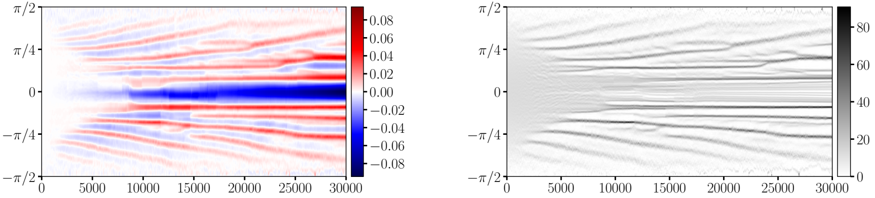

narrow band

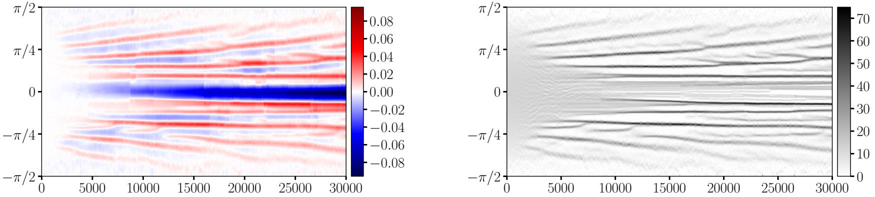

broad band

Effect of forcing spectrum: observations

No qualitative differences are seen: similar jet spacing, intensity and poleward drift.

A *retrograde* equatorial jet develops (sub-rotation).

Polar regions are highly dynamic, with no discernible jet structure.

Jets are persistently *wavy*, even though sharp.

Drifting jets?

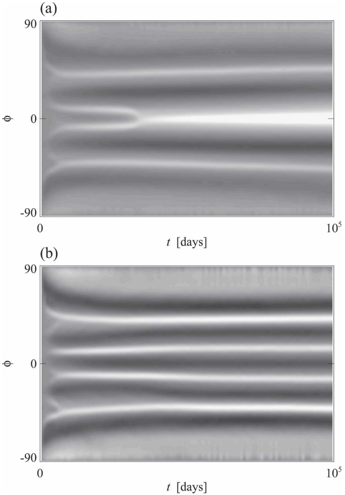

FIG. 4. Zonal velocity vs latitude and time for different forms of large-scale dissipation: (a) radiative relaxation with relaxation coefficient $\nu_l = 1$ and (b) hypodiffusion with diffusion coefficient $\nu_l = 0.01$. Energy input is the same as in Fig. 2a. Gray scale is normalized according to the rms value, with light (dark) shade indicating eastward (westward) flow.

Scott & Polvani (2007) (and others since) mainly observe steady jets, *i.e.* little or no drifting.

Notably they used vorticity forcing, rather than topographic, as here.

Many papers have followed Scott & Polvani (2007); Showman (2007) seems to be the exception.

Is topographic forcing however appropriate?:

Our forcing is designed to represent the actual forcing of the giant planetary atmospheres by overturning convective systems or other random motions generated by the deep turbulent interior. There is very little

— from Scott & Polvani (2007).

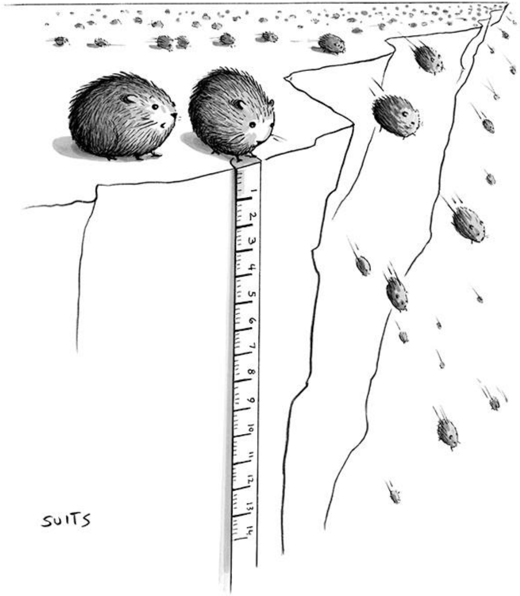

"You're overthinking this."

Effect of Rossby deformation wavenumber

$\tau = 100, \;\; b_{\mathrm{rms}} = 0.005, \;\; t_b = 50 \;\;$ (broad band)

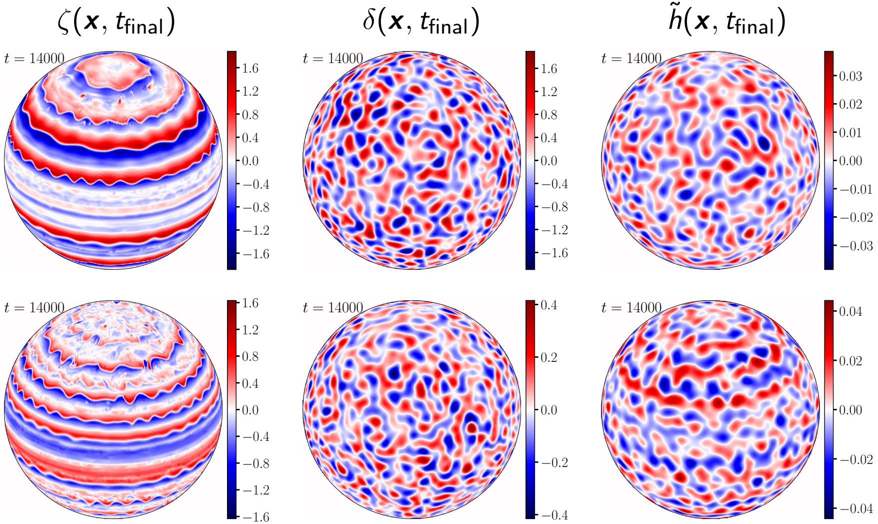

- top: $k_D = 5$
- bottom: $k_D = 25$

$\tau = 100$, $b_{\text{rms}} = 0.005$, $t_b = 50$ (broad band)

$\bar{u}(t, \phi)$ $\partial\bar{q}/\partial\phi(t, \phi)$

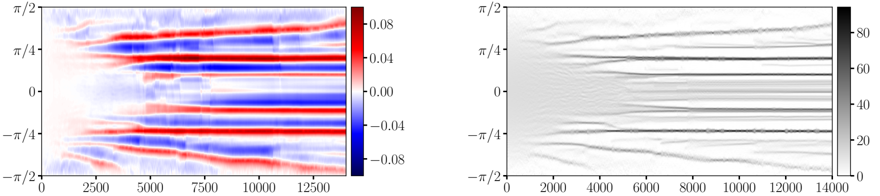

$k_D = 5$

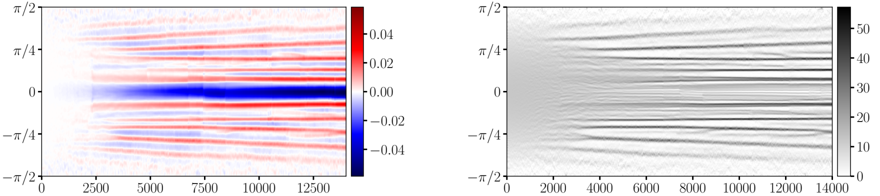

$k_D = 25$

Effect of Rossby deformation wavenumber: observations

As k_D increases, both jet spacing and intensity decrease.

Large k_D favours the development of a strong equatorial easterly flow, associated with PV homogenisation.

Only high-latitude jets drift polewards. (Here τ is five times smaller than before — stronger thermal damping.)

Divergent motions are greatly suppressed at large k_D.

Effect of thermal relaxation timescale

$k_D = 5, \ \ b_{\rm rms} = 0.005, \ \ t_b = 50 \ \ $ (broad band)

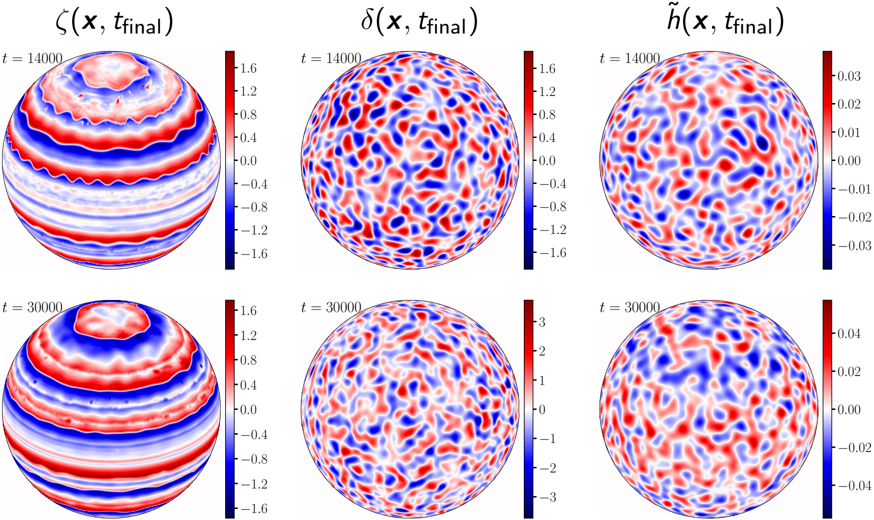

- top: $\tau = 100$
- bottom: $\tau = 500$

$k_D = 5, \;\; b_{\rm rms} = 0.005, \;\; t_b = 50 \;\; \text{(broad band)}$

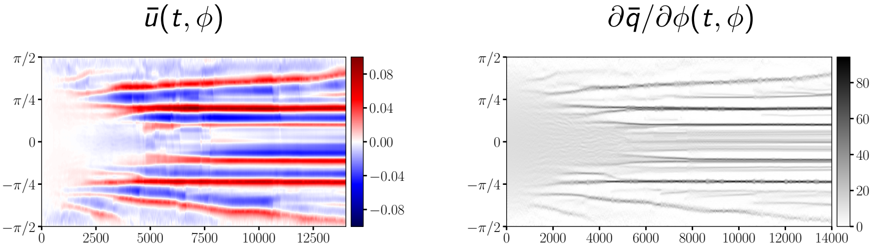

$\tau = 100$

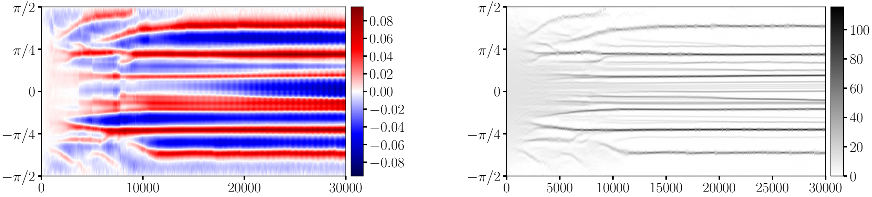

$\tau = 500$

$k_D = 5, \quad \tau = 500, \quad b_{\mathrm{rms}} = 0.005, \quad t_b = 50 \quad$ (broad band)

Jet structure at the final time, $t = 30000$

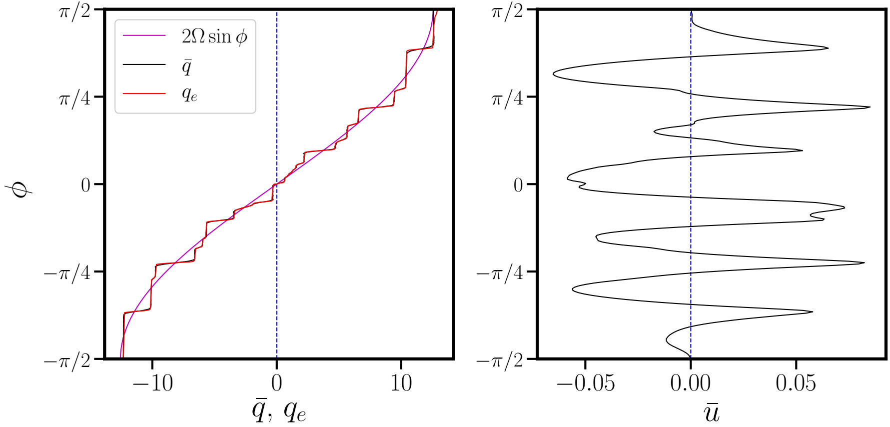

$k_D = 25$, $b_{\text{rms}} = 0.005$, $t_b = 50$ (broad band)

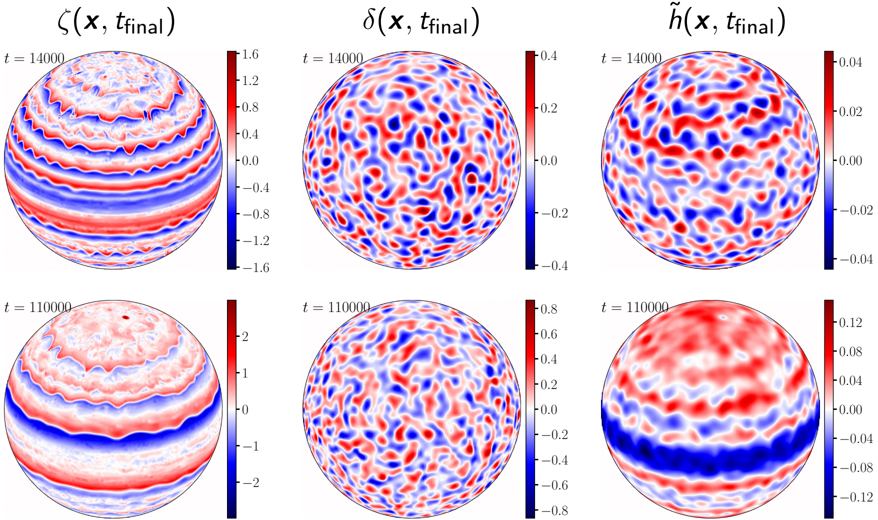

- top: $\tau = 100$
- bottom: $\tau = 2500$

$k_D = 25, \quad b_{\mathrm{rms}} = 0.005, \quad t_b = 50 \quad$ (broad band)

$\bar{u}(t,\phi)$ $\qquad$ $\partial\bar{q}/\partial\phi(t,\phi)$

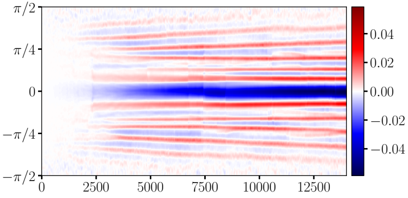

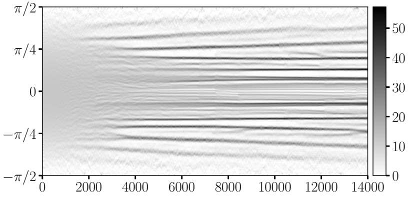

$\tau = 100$

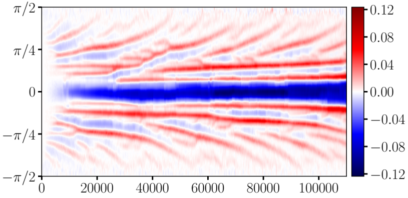

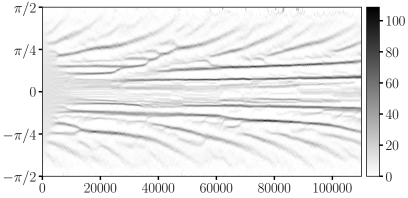

$\tau = 2500$

Effect of thermal relaxation timescale: observations

Only small k_D and large τ produce "locked-in" jets across all latitudes.

Strong equatorial easterlies develop for large k_D, regardless of the thermal damping timescale.

For large k_D and τ, the fluid layer bulges in polar regions and dips near the equator.

Divergent motions increase with τ.

Effect of forcing de-correlation timescale

$k_D = 5, \;\; \tau = 500, \;\; b_{\text{rms}} = 0.005 \;\; \text{(broad band)}$

$\zeta(\boldsymbol{x}, t_{\text{final}})$ $\delta(\boldsymbol{x}, t_{\text{final}})$ $\tilde{h}(\boldsymbol{x}, t_{\text{final}})$

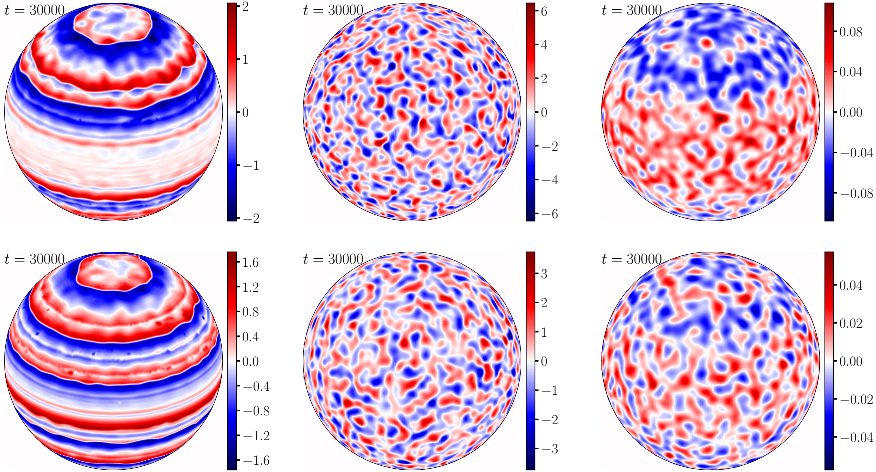

- top: $t_b = 10$
- bottom: $t_b = 50$

$k_D = 5, \;\; \tau = 500, \;\; b_{\rm rms} = 0.005$ (broad band)

$\bar{u}(t, \phi)$ $\qquad$ $\partial \bar{q}/\partial \phi(t, \phi)$

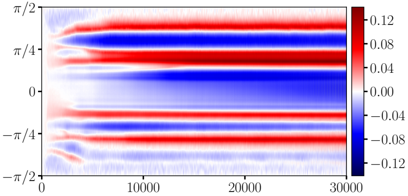

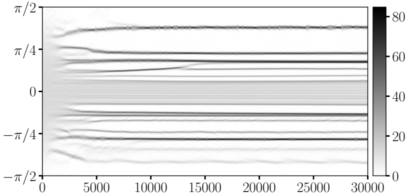

$t_b = 10$

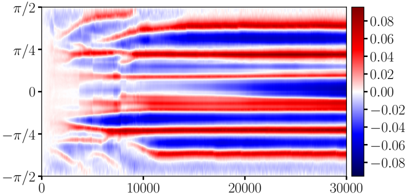

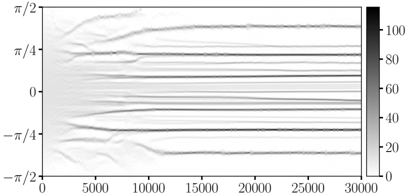

$t_b = 50$

Effect of forcing de-correlation timescale: observations

As t_b decreases, the jets appear to become more steady.

But, divergent motions increase and become smaller-scale.

Also, the fluid layer dips in polar regions and bulges near the equator.

Furthermore, jets are excluded from the equatorial region; only a wide easterly flow is observed.

Effect of forcing amplitude

$k_D = 25, \;\; \tau = 500, \;\; t_b = 50$ (narrow band)

$\zeta(\boldsymbol{x}, t_{\mathrm{final}})$ $\delta(\boldsymbol{x}, t_{\mathrm{final}})$ $\tilde{h}(\boldsymbol{x}, t_{\mathrm{final}})$

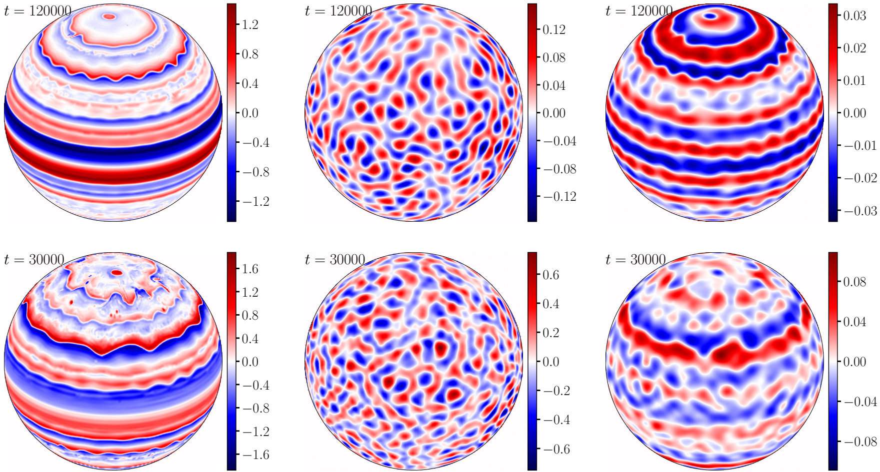

- top: $b_{\mathrm{rms}} = 0.001$
- bottom: $b_{\mathrm{rms}} = 0.005$

$k_D = 25, \;\; \tau = 500, \;\; t_b = 50 \;\;$ (narrow band)

$\bar{u}(t,\phi)$ $\qquad$ $\partial\bar{q}/\partial\phi(t,\phi)$

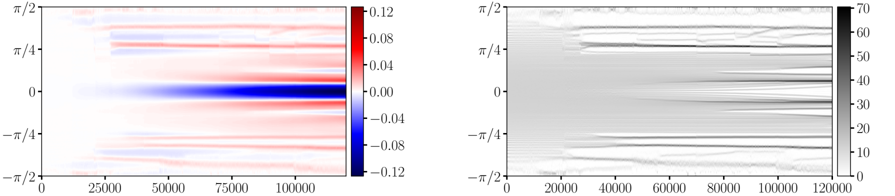

$b_{\mathrm{rms}} = 0.001$

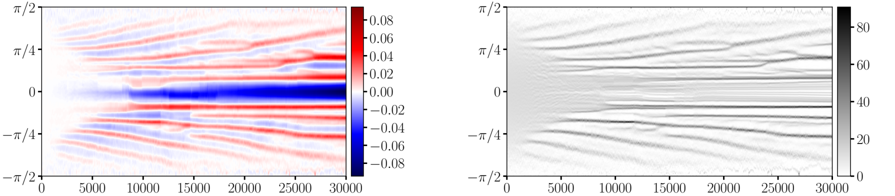

$b_{\mathrm{rms}} = 0.005$

$k_D = 25,\ \ \tau = 500,\ \ b_{\rm rms} = 0.001,\ \ t_b = 50$ (narrow band)

Jet structure at the final time, $t = 120000$

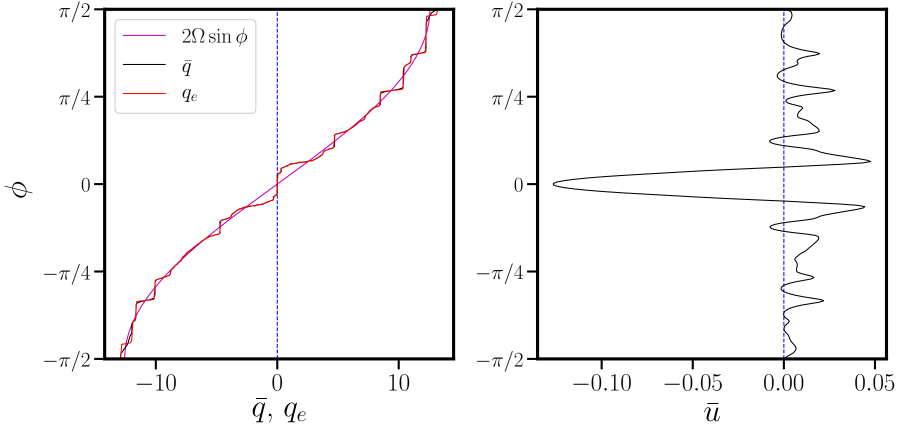

Effect of forcing amplitude: observations

As $b_{\rm rms}$ decreases, the jets emerge more slowly, are weaker and less wavy.

Also, jets form more readily in mid-latitude and polar regions and are visible in the height anomaly $\tilde{h}$.

A strong *retrograde* equatorial jet develops (sub-rotation).

The jets are more steady — they exhibit little drift.

Furthermore, divergence is much weaker. Vorticity now dominates.

Conclusions: Part 1 of 2

- We have revisited jet formation in forced spherical shallow-water flows.

- The vorticity forcing introduced by Scott & Polvani (2007) — and used by many others since — mainly excites balanced, PV-controlled motions, e.g. Rossby waves.

- Like Showman (2007), we use "topographic" forcing to mimic the effects of convection.

- Such forcing results in retrograde equatorial jets (sub-rotation) in all cases, *contrary* to what was found by Saito & Ishioka (2015) and many others:

> value of latitude for Rossby modes. To summarize, the essential cause of the prograde acceleration at the equator in a shallow-water system with Newtonian cooling is the latitudinal dependence of the dissipation acting on the Rossby modes. This implies that equatorial superrotation

Conclusions: Part 2 of 2

- Topographic forcing excites *imbalanced* inertia–gravity waves **much more strongly** than the vorticity forcing used in nearly all past studies.

- The numerical algorithm has *exceptionally weak* numerical damping, enabling inertia–gravity waves to have a much greater impact.

- Another major difference is that topographic forcing often leads to poleward jet drift.

- Exceptions occur for very weak forcing, or for a low to moderate Rossby deformation wavenumbers.